Solid-State Transfer Switch Topologies for a Switched Doubly Fed Machine Drive

Arijit Banerjee, *Student Member, IEEE*, Steven B. Leeb, *Fellow, IEEE*, and James L. Kirtley Jr., *Life Fellow, IEEE*

***Abstract*—Switched doubly fed machines (DFM) enable the creation of variable speed drives with reduced power electronics requirements compared to shaft power, and with the additional benefit of controllable stator power factor. A transfer switch is a critical component of a switched-DFM drive, permitting reconfiguration of the stator power connections. A solid-state transfer switch not only allows seamless shaft control across the full-speed range but also permits effective grid interaction. This paper presents and compares different transfer switch topologies that can reconfigure the DFM connections on-the-fly as shaft speed demands vary. Constraints on operating conditions are derived that can allow DFM mode transitions without any additional commutation circuitry. Experiments demonstrate the performance of the transfer switch under different operating conditions.**

***Index Terms*—Doubly fed machine, high power, microgrid, natural commutation, propulsion drive, solid-state transfer switch, short-circuit ratio (SCR), wide-speed range.**

I. Introduction

HIGH-POWER variable speed drives (VSD) have wide range of applications in industrial processes, electric propulsion systems, and power generation plants [1]. Most VSDs require power converters rated to handle the full shaft power. Power flow is controlled by the converter to different electrical machine types depending on the drive, including permanent magnet [2], squirrel-cage induction [3], wound-rotor induction [4], and synchronous types [5]. Typically, the power electronic drive design is limited by the available component ratings and allowable device switching frequency. For example, at present, the voltage rating of the typical IGBTs that are available for medium voltage drives ranges between 3.3 to 6.5 kV with an allowable switching frequency of a few hundred Hz [6]. Often multiple devices are stacked in series/parallel as in the multilevel converters [7]–[11] or the electrical machine is designed with more than three phases as in [12]. This has led to a considerable effort from research to product development focusing on different topologies and combinations of multilevel converters and multiphase machines [13]–[15].

Of the four machine types typically available for high-power applications, permanent magnet, squirrel-cage induction, and synchronous machines are inherently configured with a single electrical port and a single mechanical port for power transfer. For these machines configured as VSDs, a power converter connected in series with the electrical port of the machine must be rated at the shaft power to control the electromechanical energy conversion. However, a wound-rotor induction/doubly fed machine (DFM) has two accessible electrical ports to control energy conversion, adding flexibility in the drive design. This flexibility has been widely used in limited-speed range applications, such as in the wind power generation [16]. For full-speed range applications, including electric propulsion drives, the flexibility of the DFM can be exploited with on-the-fly reconfiguration of the power connections to the stator—a configuration known as a switched-DFM drive [17]. A typical switched-DFM drive operates over a speed range of ± 1.5 p.u. (normalized relative to the ac source synchronous speed) with a rotor converter power rating of a third of the maximum shaft power [18]. The reduction in the converter rating improves drive efficiency, reduces filter size, lowers the fundamental drive frequency, improves machine-side and source-side harmonics, and reduces converter cooling requirements [19]. Additionally, the switched-DFM drive offers seamless interface, controllable power factor, and reactive power support to the ac grid [20]. Fig. 1 shows a switched-DFM drive with a transfer switch that connects the stator windings of the DFM to multiple sources or shorts the stator windings together while a back-to-back power converter controls the electromechanical energy conversion from the rotor winding.

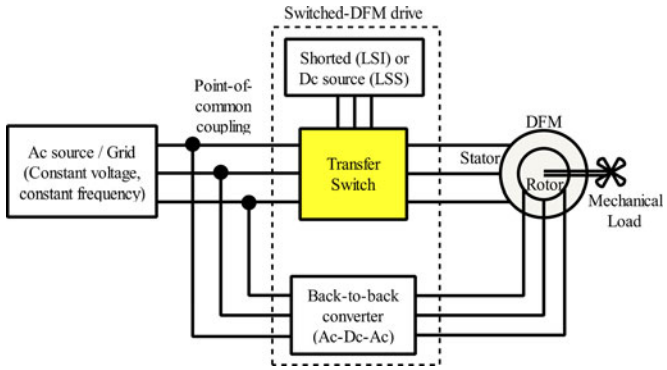

Fig. 1. Typical configuration of a switched-DFM drive.

Depending on the possible stator winding reconfigurations, the switched-DFM drive can operate either in the low-speed induction topology (LSI) or in the low-speed synchronous topology (LSS) [21]–[23]. At lower drive speed, the DFM stator is shorted in the LSI topology or is connected to a low-voltage dc source in the LSS topology. This mode of operation of

Manuscript received June 8, 2015; accepted October 5, 2015. Date of publication October 12, 2015; date of current version March 2, 2016. This work was supported by the Skoltech-MIT SDP Program, the Kuwait Foundation for the Advancement of Sciences (KFAS) through the Kuwait-MIT Center for Natural Resources and the Environment (CNRE), and The Grainger Foundation. Recommended for publication by Associate Editor S. K. Panda.

The authors are with the Department of Electrical Engineering and Computer Science, Massachusetts Institute of Technology, Cambridge, MA 02139 USA (e-mail: arijit@mit.edu; sbleeb@mit.edu; kirtley@mit.edu).

Color versions of one or more of the figures in this paper are available online at http://ieeexplore.ieee.org.

Digital Object Identifier 10.1109/TPEL.2015.2489463

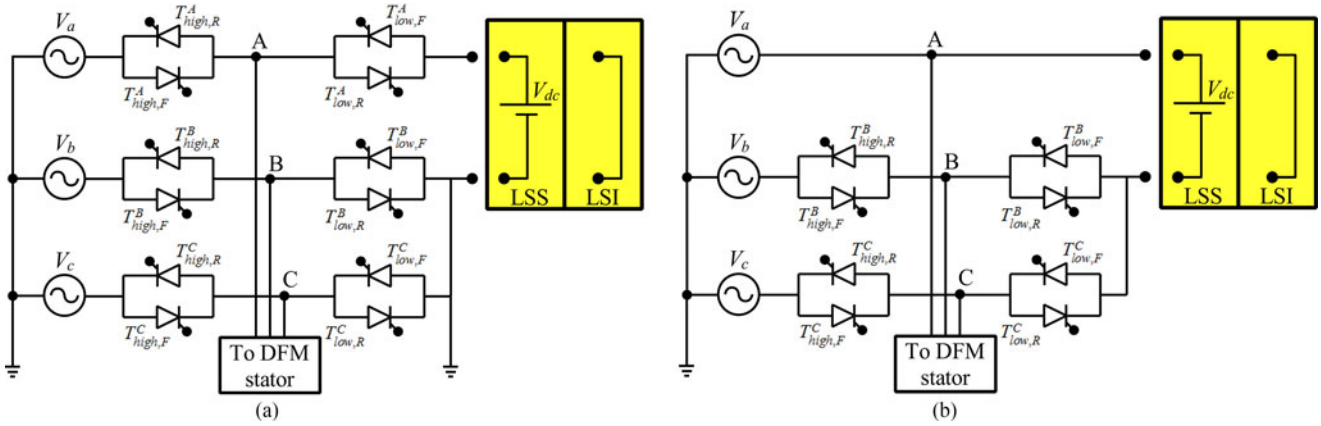

Fig. 2. SCR-based transfer switch topologies. (a) TTB—The neutral of the ac source voltage is the reference for the transfer switch operation. [26] (b) ETB—A phase of the ac source is the reference for the transfer switch operation.

the switched-DFM drive is referred to as "low-speed" mode. At higher drive speed, in both topologies, the DFM stator is connected to the ac source/grid, which is denoted as "high-speed" mode. The mode transition speed depends on the topology as well as on the required drive torque–speed characteristic.

The transfer switch is the most critical component in a switched-DFM drive. Although a mechanical transfer switch can potentially be used for the stator reconfiguration [21], [24], [25], this choice results in poorer reliability and transfer performance for applications that need frequent reconfigurations and seamless performance at all speeds. Of course, for all of the configurations shown in this paper, a mechanical transfer switch could be used in parallel with a semiconductor transfer switch to reduce steady-state losses to a minimum. Banerjee *et al.* [26] proposed a twelve-thyristor-based (TTB) transfer switch that offers seamless transition and drive performance with an appropriate rotor-side control [27]. However, there are other design options in making a thyristor (SCR)-based transfer switch. This paper presents alternative configurations of the SCR-based transfer switch using eight thyristors. Constraints on the ac source voltage are derived during the mode transition for a natural commutation of the outgoing SCRs and a seamless transition from the DFM perspective. Analysis and evaluations are presented to compare and contrast the performance of these transfer switch options in achieving a seamless performance and harmonious grid interaction of the switched-DFM drive. Experimental results are presented to verify the operation of the proposed transfer switch using an off-the-shelf 1 HP, 220 V/150 V, 4 pole, 1800 r/min DFM.

II. SCR-Based Transfer Switch Topology and Operation

Different options for an SCR-based transfer switch topology that can connect the stator of the DFM to the appropriate sources or short the stator together are shown in Fig. 2. The TTB transfer switch is shown in Fig. 2(a) and can be used both in the LSI as well in the LSS topology [28]. The transfer switch topology resembles a conventional static transfer switch used in providing back-up power to critical loads from multiple ac sources [29]–[34]. Each of the antiparallel SCR modules-per-phase ensures a bidirectional current carrying and a bidirectional voltage blocking capability as required by the transfer switch. The SCR commutation requirements during mode transitions are based on the neutral of the ac source as the reference potential. The voltage rating of the SCRs has to be sufficient to withstand the ac source phase voltages.

The proposed eight-thyristor-based (ETB) transfer switch is shown in Fig. 2(b). The A phase of the DFM is permanently connected to the A phase of the ac source voltage. In high-speed mode, SCRs $T^B_{\text{high},F}$, $T^B_{\text{high},R}$, $T^C_{\text{high},F}$, and $T^C_{\text{high},R}$ are turned ON, thereby connecting the remaining two phases of the DFM stator to the ac source. These four SCRs form the high-speed SCR-bank. Each of these SCRs conduct for half of the time period corresponding to the ac source fundamental frequency. Alternatively, in low-speed mode, SCRs $T^B_{\text{low},F}$, $T^B_{\text{low},R}$, $T^C_{\text{low},F}$, and $T^C_{\text{low},R}$ are turned ON either to connect the stator to the dc source in the LSS topology or to short them together in the LSI topology. These four SCRs are collectively termed as the low-speed SCR-bank. In the LSS topology, the positive polarity of the dc source is permanently connected to the A phase of the ac source. As the dc source is created using a transformer rectifier from the ac source, there is inherent isolation between the sources. In the LSI topology, the three-phase stator windings are all connected to the A phase of the ac source voltage during low-speed operation. The SCRs used in this topology are rated to withstand ac source line-to-line voltages.

The TTB transfer switch operation has been detailed in [26]. In the following section, the operation of the ETB transfer is analyzed and compared with the operation of the TTB transfer switch. Analysis shows that the proposed configuration relaxes the constraints on the ac source voltage and the stator current for the natural commutation of the outgoing SCRs leading to a better seamless performance of the drive and more specifically under the light drive torque conditions.

A. ETB Transfer Switch: Conditions for Natural Commutation of the Outgoing SCRs

The commutation requirement for the ETB transfer switch is considered in light of the drive topology and operating mode

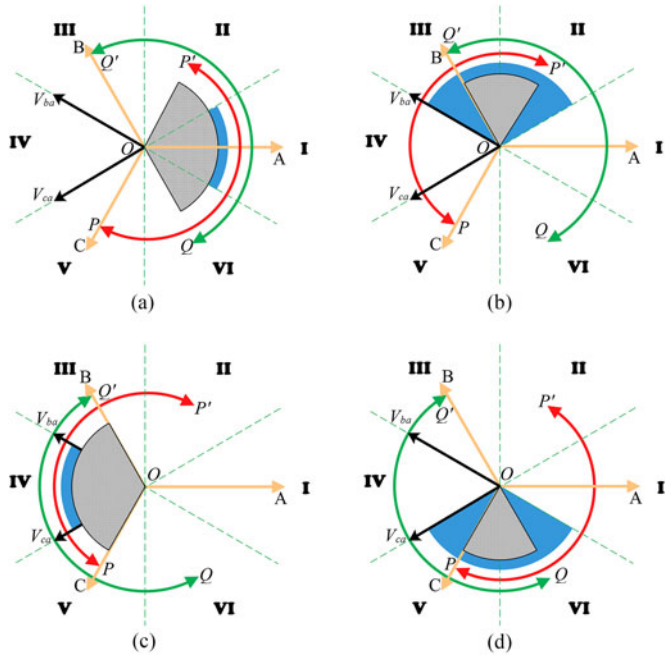

Fig. 3. Commutation diagram during low-speed-to-high-speed mode transition in the LSI topology. Red arc (PP') : allowable line-to-line voltage between B and A phase for natural commutation of the B phase SCRs. Green arc (QQ'): allowable line-to-line voltage between C and A phase for natural commutation of the C phase SCRs. Blue-filled sector: stator current vector location. Hatched sector: allowable ac source voltage vector for simultaneous natural commutation of all the outgoing SCRs. (a) Current polarities in the B and C phase are both negative (b) Current polarity in the B phase is positive while in the C phase is negative (c) Current polarities in the B and C phase are both positive (d) Current polarity in the B phase is negative while in the C phase is positive.

transition. Constraints on the ac source voltage are derived based on the DFM stator current that ensures simultaneous commutations of all the outgoing SCRs without shorting the sources or requiring any additional auxiliary circuit for SCR commutation [35].

1) LSI Topology - Commutation Requirement During Low-Speed-to-High-Speed Mode Transition: With the DFM stator initially shorted, the low-speed SCR-bank is ON and the stator current alternates at the slip frequency. Depending on the stator current polarity in the B and C phases, one of the two SCRs per phase conducts at any instant of time. This gives rise to four possible combinations for the SCR commutation requirement based on the polarity of the current in the B and C phases. The four possible combinations are demarcated in the commutation diagram by the filled-blue sectors relative to the stator ABC winding axis as shown in Fig. 3. For example, a negative polarity of stator currents in the B and C phases corresponds to the condition when the stator current vector is in sector I as shown in the Fig. 3(a).

The polarities of the incoming ac source line voltages $V_{\rm ba}$ and $V_{\rm ca}$ must be same as the polarity of the respective phase stator currents in the B and C phases to naturally steer the stator current to the ac source at the instant of mode transition. These constraints are satisfied when the incoming ac source voltage vector is within the arc PP' and QQ' respectively. The intersection of the two arcs form the hatched sector that represents the allowable region for the ac source voltage vector at the instant of mode transition for a natural commutation of the outgoing SCRs in the low-speed SCR-bank. The required constraints on the ac source voltage vector and the participating SCRs for all possible stator current vector locations have been detailed in Table I.

2) LSI Topology - Commutation Requirement During High-Speed-to-Low-Speed Mode Transition: With the DFM stator initially connected to the ac source, the high-speed SCR-bank is ON. The stator current and the ac source voltage alternate at the ac source frequency. Fig. 4 depicts the constraints on the allowable ac source voltage vector location (hatched sector) based on the stator current vector location (filled-blue sector) for simultaneous natural commutation of all outgoing SCRs. For example, a negative stator current amplitudes in the B and C phases require the ac source voltage vector to be within the sector POQ' in Fig. 4(a).

As evident from Fig. 4, ideally the stator power factor angle must be between 90° and 270° at the instant of high-speed-to-low-speed mode transition independent of the stator current polarity for a natural commutation of the outgoing SCRs in the high-speed SCR-bank. The allowable range of power factor angles for the ETB transfer switch is wider by 60° compared to the TTB transfer switch [26], [28]. The wider range of allowable stator power factor angles add more flexibility in terms of allowable reactive power and transition condition from the DFM perspective. Table I also includes the required ac source voltage vector constraint and the participating SCRs during a high-speed-to-low-speed transition for all the possible stator current vector locations.

3) LSS Topology - Effect of the dc Source on the Transfer Switch Commutation Requirement: During steady-state low-speed operation, the stator current is dc in the LSS topology. The stator A phase is connected to the positive polarity of the isolated dc source of magnitude $V_{\rm dc}$ and the B and C phases are connected to the negative polarity as shown in Fig. 2(b). The connection enforces a stationary stator current vector $\overline{I_s}$ directed along the A-phase axis as shown in Fig. 5. The negative current polarities in the stator B and C phases resembles the condition of Fig. 3(a) in the LSI topology. Accounting for the dc source voltage magnitude, the required conditions on the incoming ac source voltages for a natural commutation of the outgoing SCRs are given by

$$\begin{aligned} V_a - V_{\rm dc} &> V_b \\ V_a - V_{\rm dc} &> V_c. \end{aligned} \tag{1}$$

Rearranging (1) in terms of the ac source line-to-line voltages and the dc source voltage magnitude gives the following constraints:

$$\begin{aligned} V_{ba} &< -V_{\rm dc} \\ V_{ca} &< -V_{\rm dc}. \end{aligned} \tag{2}$$

The above constraints are shown by the lines XX' and YY' in Fig. 5. Intersection of the two constraints forms the hatched sector $P'OQ$ that sets the bound on the allowable location of

TABLE I
COMMUTATION CONSTRAINTS ON ALLOWABLE AC SOURCE VOLTAGE VECTOR LOCATION BASED ON THE LOCATION OF THE STATOR CURRENT VECTOR FOR SIMULTANEOUS NATURAL COMMUTATION OF ALL OUTGOING SCRS IN THE LSI TOPOLOGY

Stator current location	Low-speed-to-high-speed mode transition			High-speed-to-low-speed mode transition		
	Required ac-source voltage vector location	Outgoing SCRs	Incoming SCRs	Required ac-source voltage vector location	Outgoing SCRs	Incoming SCRs
Sector I	$-60^\circ < \angle\overline{V_{\rm ac}} < 60^\circ$	$T^B_{{\rm low},R}\ T^C_{{\rm low},R}$	$T^B_{{\rm high},R}\ T^C_{{\rm high},R}$	$120^\circ < \angle\overline{V_{\rm ac}} < 240^\circ$	$T^B_{{\rm high},R}\ T^C_{{\rm high},R}$	$T^B_{{\rm low},R}\ T^C_{{\rm low},R}$
Sectors II, III	$60^\circ < \angle\overline{V_{\rm ac}} < 120^\circ$	$T^B_{{\rm low},F}\ T^C_{{\rm low},R}$	$T^B_{{\rm high},F}\ T^C_{{\rm high},R}$	$240^\circ < \angle\overline{V_{\rm ac}} < 300^\circ$	$T^B_{{\rm high},F}\ T^C_{{\rm high},R}$	$T^B_{{\rm low},F}\ T^C_{{\rm low},R}$
Sector IV	$120^\circ < \angle\overline{V_{\rm ac}} < 240^\circ$	$T^B_{{\rm low},F}\ T^C_{{\rm low},F}$	$T^B_{{\rm high},F}\ T^C_{{\rm high},F}$	$-60^\circ < \angle\overline{V_{\rm ac}} < 60^\circ$	$T^B_{{\rm high},F}\ T^C_{{\rm high},F}$	$T^B_{{\rm low},F}\ T^C_{{\rm low},F}$
Sectors V, VI	$240^\circ < \angle\overline{V_{\rm ac}} < 300^\circ$	$T^B_{{\rm low},R}\ T^C_{{\rm low},F}$	$T^B_{{\rm high},R}\ T^C_{{\rm high},F}$	$60^\circ < \angle\overline{V_{\rm ac}} < 120^\circ$	$T^B_{{\rm high},R}\ T^C_{{\rm high},F}$	$T^B_{{\rm low},R}\ T^C_{{\rm low},F}$

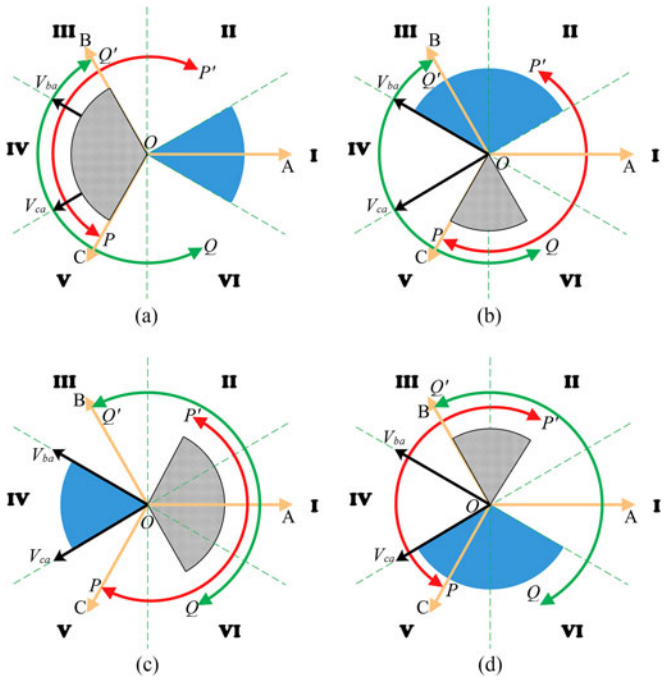

Fig. 4. Commutation diagram during high-speed-to-low-speed mode transition in the LSI topology. Red arc (PP'): allowable line-to-line voltage between B and A phase for natural commutation of the B phase SCRs. Green arc (QQ'): allowable line-to-line voltage between C and A phase for natural commutation of the C phase SCRs. Blue-filled sector: stator current vector location. Hatched sector: allowable ac source voltage vector for simultaneous natural commutation all outgoing SCRs. (a) Current polarities in the B and C phases are both negative (b) Current polarities in the B phase is positive while in the C phase is negative (c) Current polarities in the B and C phases are both positive (d) Current polarities in the B phase is negative while in the C phase is positive.

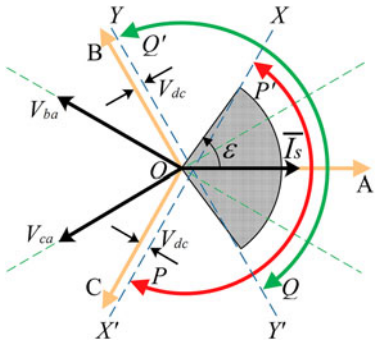

Fig. 5. Allowable ac source voltage vector location for a low-speed-to-high-speed mode transition in the LSS topology of the switched-DFM drive. Prior to mode transition, the stator current vector is stationary and aligned with the stator A-phase axis. The allowable sector boundary incorporates the necessary constraints due to the presence of the dc source voltage.

the incoming ac source voltage vector for a successful natural steering of the stator current from the dc source to the ac source.

The angle ϵ of the sector $P'OQ$ in Fig. 5 is dependent on the voltage magnitude of the dc source and the line-to-line voltage of the ac source and is given by

$$\varepsilon = 60^\circ - \arcsin\frac{V_{\rm dc}}{V_{\rm ab}}. \tag{3}$$

For example, for a dc source of 20-V magnitude and an ac source of 146-V (rms, line-to-line), the incoming ac voltage vector must be within $\pm 55.5^\circ$ relative to the stator A-phase winding axis for a simultaneous natural commutation of SCRs $T^B_{{\rm low},R}$ and $T^C_{{\rm low},R}$ during low-speed-to-high-speed mode transition. In the TTB transfer switch, the equivalent allowable sector angle is $\pm 30^\circ$ [26]. The extension in the allowable stator voltage vector location helps in reducing the stator flux transients and shaft torque perturbation particularly during mode transition with a low-drive-torque demand as will be shown in Section II-B2.

The high-speed-to-low-speed mode transition in the LSS topology has identical constraints on the ac source voltage vector as outlined for the LSI topology in Section II-A2. However, the sector boundaries need to be adjusted to incorporate the presence of the dc source voltage in a similar manner.

B. Constraints on the SCR-Based Transfer Switch Operation from the DFM Perspective

Having determined the allowable ac source voltage vector location for natural commutation of the outgoing SCRs, this section superimposes the requirement from the DFM perspective that will ensure a seamless mode transition with respect to the shaft torque and speed. A synchronizer governs the correct transition instant for a seamless reconfiguration of the DFM. Conditions have been derived for the synchronizer that can minimize the perturbation in the DFM state variables during the mode transition for both the LSS topology [27] and the LSI topology [28]. In this section, the synchronizer operation is evaluated within the constraints of the natural commutation of the outgoing SCR-bank for the ETB transfer switch.

1) LSI Topology - Low-Speed-to-High-Speed Mode Transition: There are two criteria to be satisfied by the synchronizer

for a bump-less low-speed-to-high-speed mode transition. First, assuming a *d–q* reference frame oriented to the stator flux, the *d*-axis component of the incoming ac voltage vector must be aligned with the existing *d*-axis stator voltage prior to the mode transition. Second, the *q*-axis component of the incoming ac source voltage must be a positive quantity. Prior to mode transition, the stator voltage is zero due to the shorted configuration. With no source of magnetizing current from the stator side, the stator current vector is always orthogonal to the stator flux vector. A positive drive torque implies that the stator current vector leads the stator flux vector by 90°.

Based on the synchronizer requirement, for a positive drive torque, the incoming ac source voltage vector must be aligned with the stator current vector for a seamless low-speed-to-high-speed mode transition [28]. This requirement is achievable along with simultaneously satisfying the commutation constraints for the outgoing SCRs for the proposed transfer switch for all the conditions where the filled-blue sectors overlap with the hatched sectors in the commutation diagrams of Fig. 3. While the overlapping of the two sectors forms the major share of the fundamental ac cycle, there exists, however, four sub-sectors 30° to 60°, 120° to 150°, 210° to 240°, and 300° to 330° in the commutation diagram when both the conditions of minimal stator flux perturbation and natural commutation of the outgoing SCR cannot be simultaneously satisfied. If the stator current vector is located within these four forbidden sectors at the instant, a mode transition is demanded, either the transition has to be delayed such that the stator current vector is outside of these sectors or a nonoptimum transition instant has to be chosen to satisfy the natural commutation requirement. If the drive torque command during the low-speed-to-high-speed mode transition is negative, the synchronizer requirement and the natural commutation requirement cannot be satisfied simultaneously. However, in most of the operating scenarios, a low-speed-to-high-speed mode transition implicitly requires a nonzero positive drive torque.

2) LSS Topology - Low-Speed-to-High-Speed Mode Transition: In the LSS topology, the two criteria of the synchronizer can be simultaneously satisfied along with the commutation constraint for the outgoing SCRs for a high-positive-drive-torque demand. However, satisfying all the requirements during a low-drive-torque demand becomes challenging. This is illustrated using Fig. 6. The angle between the stationary stator flux vector $\overline{\psi_{\rm sdc}}$ and the stator current vector $\overline{I_s}$ is denoted by δ. The angle δ is proportional to the drive torque. Under low-drive-torque demand with a relatively smaller δ, matching the *d*-axis component of the dc source stator voltage vector $\overline{V_{\rm dc}}$ to the *d*-axis component of the incoming ac source voltage vector and ensuring a positive *q*-axis component leads $\overline{V_{\rm ac}}$ to be the ideal instant for the low-to-high-speed mode transition. However, the ac voltage vector $\overline{V_{\rm ac}}$ lies outside the allowable region for simultaneous natural commutation of the outgoing SCRs in the B and C phases. Under such scenario, satisfying the condition for the natural commutation of the outgoing SCRs is given priority and the mode transition is initiated at the boundary of the commutation constraint, which in this case corresponds to the ac voltage vector location $\overline{V'_{\rm ac}}$. This leads to a nonoptimum transition from the DFM perspective resulting in additional oscillation in the stator flux magnitude. The lightly-loaded rotor-side converter under low-drive-torque demand can be used to damp the oscillations through appropriate rotor *d*-axis current command [27].

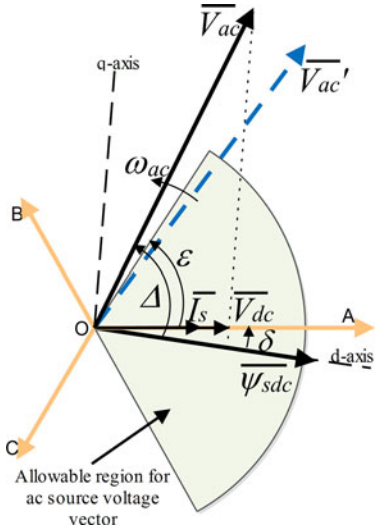

Fig. 6. Superposition of the DFM constraint on the region of allowable ac source voltage vector location for a seamless transition from the perspective shaft torque/speed. Under low-drive-torque demand, the mode transition is initiated when the ac source voltage vector is within the allowable region, at $\overline{V'_{\rm ac}}$, even though it is not an optimum transition instant, which is $\overline{V_{\rm ac}}$ from the DFM perspective.

The boundary that defines a low-drive-torque demand for the proposed transfer switch is obtained when the synchronizer requirement and the commutation constraints are marginally satisfied and is given by

$$\begin{aligned} |\overline{V_{\rm dc}}|\cos\delta_{\rm min} &= |\overline{V_{\rm ac}}|\cos\Delta \\ \Delta - \delta_{\rm min} &= \epsilon. \end{aligned} \tag{4}$$

Solving the two equations in (4) for $\delta_{\rm min}$ gives

$$\delta_{\rm min} = \arctan\left[\frac{1}{\sin\epsilon}\left(\cos\epsilon - \frac{|\overline{V_{\rm dc}}|}{|\overline{V_{\rm ac}}|}\right)\right]. \tag{5}$$

For example, with a dc source voltage 20 V and an ac source voltage 146 V (rms, line-line), the boundary of the low-drive torque is achieved when $\delta_{\rm min} = 28^\circ$. For the same dc and ac source voltage magnitudes, the equivalent boundary in the TTB transfer switch corresponds to $\delta_{\rm min} = 56^\circ$. This implies that the proposed transfer switch enables optimum transition from the DFM perspective along with the natural commutations of the SCRs for even lighter load compared to that by the TTB transfer switch. The minimum torque below which the demanded drive torque is termed "low" can be written in terms of the stator flux magnitude $|\overline{\psi_{\rm sdc}}|$, stator current vector magnitude $|\overline{I_s}|$, and the number of pole of the DFM P as

$$\tau_{\rm dc,min} = \frac{3}{2}\frac{P}{2}|\overline{\psi_{\rm sdc}}||\overline{I_s}|\sin\delta_{\rm min}. \tag{6}$$

3) LSI and LSS Topology - High-Speed-to-Low-Speed Mode Transition: During high-speed-to-low-speed mode transition, for an ideal DFM with a sinusoidal stator current and ac source

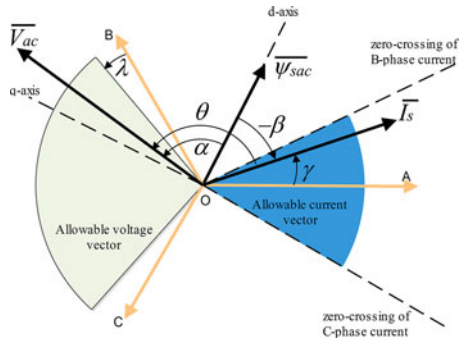

Fig. 7. High-speed-to-low-speed mode transition: Incorporating safety margins on the allowable location of the ac source voltage vector location and current vector location for guaranteed mode transition in the presence of nonidealities of the DFM and noise and harmonics in the source waveforms.

voltage, any negative drive torque command can achieve a power factor angle between 90° and 270° to satisfy the commutation requirement of the high-speed SCR-bank. However, in practice, a margin is required to accommodate the nonidealities of the DFM and the effect of noise and harmonics of the stator voltage and current waveforms. Discrepancies on the source voltages and currents from an ideal sinusoidal waveform, particularly near the zero crossings, can lead to a shorting of the sources. To enforce the margin, it is ensured that the voltage across the incoming thyristor is greater than a threshold voltage v_{th} and the current through the outgoing thyristor is greater than a threshold current i_{th} at the instant of mode transition. The threshold voltage is represented in normalized form relative to the peak ac source phase voltage while the threshold current is specified as a normalized quantity with respect to the peak rated stator current.

As an example, a high-speed-to-low-speed mode transition is considered with the stator current polarities in the B and C phases being negative. This is represented in Fig. 7. The stator current vector $\overline{I_s}$ and the ac voltage vector $\overline{V_{\text{ac}}}$ are placed to satisfy the commutation constraint required for the transition. The threshold voltage constraint for the thyristors is incorporated by specifying the bounds on the allowable ac source voltage vector as

$$120^\circ - \lambda < \theta + \gamma < 240^\circ + \lambda \tag{7}$$

where

$$\lambda = \arcsin\left(\frac{v_{th}}{\sqrt{3}}\right)$$

γ is the angle between the stator current vector and the stator A-phase axis, and θ is the stator power factor angle. The stator current vector angle is bounded by

$$-30^\circ < \gamma < 30^\circ. \tag{8}$$

The threshold current constraint is incorporated by specifying the bounds on the allowable stator B- and C-phase currents at the instant of mode transition by

$$\begin{aligned} |i_b| &= |i_s \cos(120^\circ - \gamma)| > i_{th} \\ |i_c| &= |i_s \cos(240^\circ - \gamma)| > i_{th} \end{aligned} \tag{9}$$

where i_b and i_c are the normalized stator currents through the thyristors $T^B_{\text{high},R}$ and $T^C_{\text{high},R}$, respectively. i_s is the normalized stator current magnitude.

With the d-q reference frame oriented to the stator flux vector, the relationship between the stator voltage components (v_{sd}, v_{sq}), stator current components (i_{sd}, i_{sq}), and the stator flux magnitude ψ_s in the normalized form is given by

$$\begin{aligned} v_{\text{sd}} &= r_s i_{\text{sd}} \\ v_{\text{sq}} &= \psi_s + r_s i_{\text{sq}} \\ v_{\text{sd}}^2 + v_{\text{sq}}^2 &= 1 \\ i_{\text{sd}}^2 + i_{\text{sq}}^2 &= i_s^2 \end{aligned} \tag{10}$$

where r_s is the normalized stator resistance. The stator current components are related to the rotor current components (i_{rd}, i_{rq}) according to

$$\begin{aligned} \psi_s &= x_s i_{\text{sd}} + x_m i_{\text{rd}} \\ 0 &= x_s i_{\text{sq}} + x_m i_{\text{rq}} \end{aligned} \tag{11}$$

where x_s and x_m are the normalized stator and mutual inductances, respectively. The drive torque τ is given by

$$\tau = -\frac{x_m}{x_s}\psi_s i_{rq}. \tag{12}$$

The stator and the rotor currents of the DFM must be within the rated values, which in normalized form can be represented as

$$\begin{aligned} i_s^2 &\le 1 \\ i_{\text{rd}}^2 + i_{rq}^2 &\le I_{\text{rpu}}^2 \end{aligned} \tag{13}$$

where I_{rpu} is the normalized rated rotor current reflected to the DFM stator winding. For specific values of rotor current components that satisfy the constraints of (13), the stator flux magnitude can be computed by solving (10) and (11) as

$$\left(r_s\frac{\psi_s - x_m i_{rd}}{x_s}\right)^2 + \left(\psi_s - r_s\frac{x_m}{x_s}i_{\text{rq}}\right)^2 - 1 = 0. \tag{14}$$

Knowledge of the stator flux magnitude is used to calculate the components of the ac source voltage and stator current using (10) and (11), respectively. Finally, the stator power factor angle is computed by

$$\theta = \arctan\frac{v_{\text{sq}}}{v_{\text{sd}}} - \arctan\frac{i_{\text{sq}}}{i_{\text{sd}}}. \tag{15}$$

Therefore, for a specific rotor q-axis current i_{rq}, the range of rotor d-axis current i_{rd} that satisfy the constraints in (7), (8), (9), and (13) can be computed using (10), (11), (14), and (15).

For example, setting a current threshold magnitude of 0.2 p.u. and a voltage threshold magnitude of 0.1 p.u. for the example DFM, the allowable rotor current components that ensure a natural commutation of the high-speed SCR-bank is shown by area $ABCD$ in the i_{rd}–i_{rq} plane in the top trace of Fig. 8. The allowable range of i_{rq} being all positive implies that a braking torque must be commanded to the drive during the high-speed-to-low-speed mode transition, as given by (12). The corresponding magnitude is plotted on the secondary axis. The segment BC

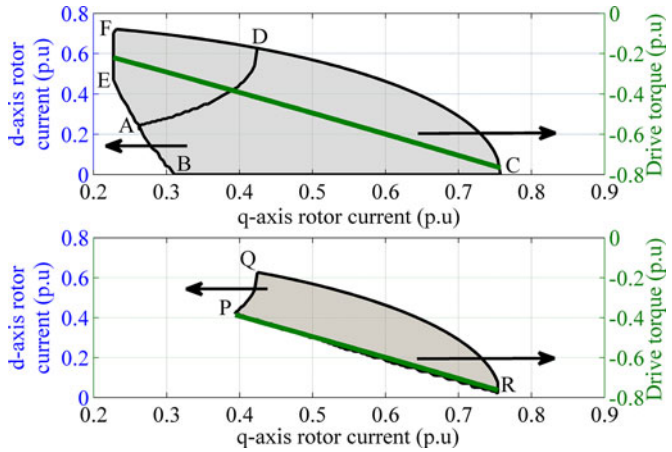

Fig. 8. Allowable rotor current components $(i_{\mathrm{rd}}, i_{\mathrm{rq}})$ that simultaneously satisfy the SCR commutation requirement and maintains a voltage higher than a threshold of 0.1 p.u. across the incoming SCRs and a current higher than a threshold of 0.2 p.u. through the outgoing SCRs at the instant of mode transition. These constraints ensure a safety margin during high-speed-to-low-speed mode transition in the presence of DFM nonidealities and noise and harmonics in the source waveforms. (Top) ETB transfer switch. (Bottom) TTB transfer switch.

represents the nonnegative bound on i_{rd} that prevents unnecessary circulating reactive power in the DFM. The segment CD represents the bound on the rotor current magnitude based on the rating of the rotor winding. As for the example DFM, the rotor current rating is lower than the stator current rating. Satisfying the rotor current constraint naturally meets the constraint of the stator current rating. The segments AB and DA represent the boundary of satisfying the threshold voltage and current constraint of the thyristors.

Alternatively, the commutation constraint can also be satisfied with the stator current in the B phase being positive and that of the C phase being negative as represented in Fig. 4(b). The above procedure can be repeated to obtain the allowable operating condition of the rotor current components by suitably modifying the bounds on λ and γ as

$$\begin{aligned} 240^\circ - \lambda \ &< \theta + \gamma < 300^\circ + \lambda \\ 30^\circ \ &< \gamma < 150^\circ. \end{aligned} \tag{16}$$

These constraints extend the allowable rotor current components by additional area $ADEF$. The remaining two possible polarity combinations of the B phase and C phase currents are within the area of $ABCDEF$.

The bottom trace of Fig. 8 shows the allowable $(i_{\mathrm{rd}}, i_{\mathrm{rq}})$ under identical voltage and current thresholds for the TTB transfer switch. The area PQR is obtained following the same procedure as the ETB transfer switch except by modifying the bounds on λ and γ as [26]:

$$\begin{aligned} 150^\circ - \lambda < \ \theta + \gamma &< 210^\circ + \lambda \\ -30^\circ < \ \gamma &< 30^\circ. \end{aligned} \tag{17}$$

Comparing the allowable regions in the i_{rq}–i_{rd} plane between the ETB transfer switch and the TTB transfer switch, it is evident that the proposed transfer switch has more flexibility in terms of operating region during the high-speed-to-low-speed mode transition. The proposed transfer switch can operate at a lower braking torque during mode transition compared to the TTB transfer switch. For the chosen voltage and current threshold, the minimum braking torque required during the high-speed-to-low-speed mode transition is 33% of the full braking torque in the proposed transfer switch. Alternatively, in the TTB transfer switch, the minimum braking torque required is 50% of the full braking torque. The required minimum braking torque influences the drive torque and the shaft speed transients during a gradual deceleration of the drive. Moreover, a wider allowable i_{rd} implies that the drive can provide an extensive reactive power support to the ac grid with an opportunity to transition to low-speed mode, if required. Finally, in the proposed transfer switch, the rotor *d*-axis current command can be set to zero for any braking torque higher than 40% of the maximum braking torque without violating the commutation constraint of the high-speed SCR-bank.

III. Alternative Eight-Thyristor-Based Transfer Switch Configuration

The transfer switch configuration proposed in Fig. 2(b) assumes that the A phase of the ac source is the reference phase for the transfer switch. Alternatively, the B and C phases of the ac source can also be chosen as the reference phase. The choice of reference phase does not influence the transition requirement and constraints for the LSI topology due to symmetricity of the shorted-stator configuration. However, it is important to consider the implications of the alternative possibilities of the transfer switch configuration for the LSS topology.

The eight SCRs can be configured between the ac and the dc sources in the LSS topology by choosing either B or C phase as the reference as shown in Fig. 9. With the DFM initially operating in low-speed mode, the stationary stator current vector $\overline{I_s}$ is aligned with the stator A-phase axis irrespective of the choice of reference phase as shown in Fig. 10. Based on the stator current vector and the reference phase, the allowable region for the ac source voltage vector for a natural commutation of the low-speed SCR-bank is shown by the hatched sector. The location of the hatched sector with the B phase as the reference can simultaneously satisfy the DFM constraints for a seamless transition as shown in Fig. 10(a). However, the location of the hatched sector with the C phase as reference is not at all suitable for a seamless transition from the perspective of the DFM under any drive torque demand as shown in Fig. 10(b).

Considering the conduction losses in the transfer switch, the A-phase reference configuration is still preferable over the B-phase reference. In low-speed mode, the stator current in A phase is twice that of the stator current in B and C phases for a balanced stator winding of the DFM. Therefore, placing an SCR on the A phase not only needs a higher current rating but also incurs higher conduction loss. In conclusion, the transfer switch topology with the A phase as reference has better performance in terms of losses and seamless mode transition compared to the other two choices in the LSS topology.

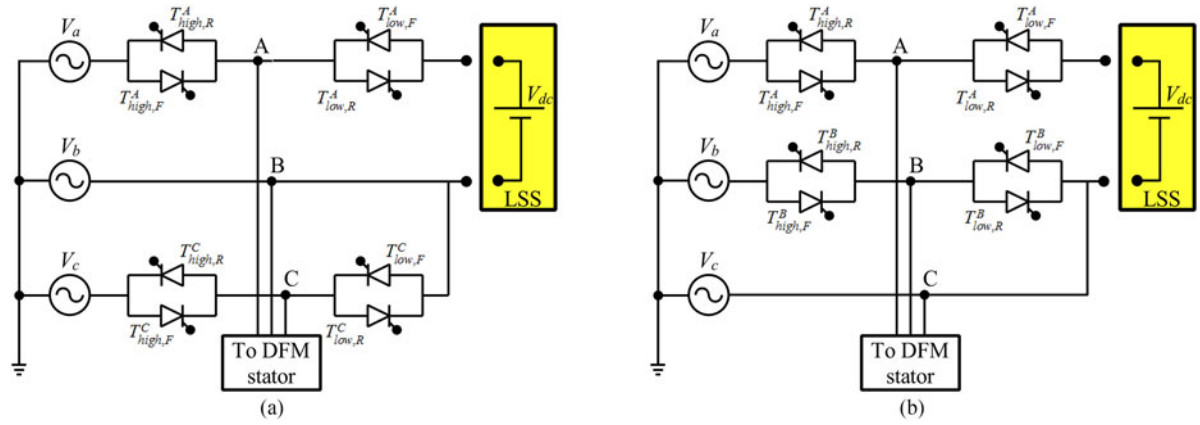

Fig. 9. Alternative configuration for the ETB transfer switch for the LSS topology. (a) B phase of the ac source is the reference for the transfer switch. (b) C phase of the ac source is the reference for the transfer switch.

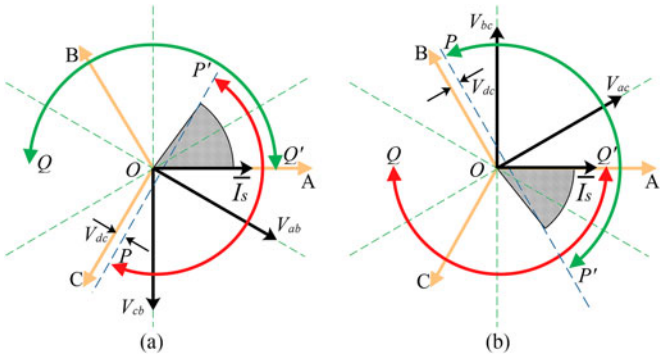

Fig. 10. Allowable ac source voltage vector location (hatched regions) in the LSS topology for alternative configuration of ETB transfer switch. (a) B phase of the ac source is the reference for the transfer switch. (b) C phase of the ac source is the reference for the transfer switch.

TABLE II
EXAMPLE DFM MACHINE PARAMETERS

DFM Parameters	
Stator resistance	3.575 Ω
Rotor resistance	4.229 Ω
Stator leakage inductance	9.6 mH
Rotor leakage inductance	9.6 mH
Mutual inductance	165 mH
Moment of inertia	0.01 kgm^2
Frictional coefficient	0.0025 Nm − s/rad
PMSG Parameters	
Back emf constant	0.1061 V-s/rad
Stator resistance	0.5 Ω

IV. EXPERIMENTAL RESULTS

The experimental setup used to verify the operation of the proposed transfer switch is shown in Fig. 11. The 146 V (line-to-line, rms), 40-Hz ac grid is created using two parallel-operated synchronous generators that provide overall power to the switched-DFM drive. The grid voltage and frequency is chosen such that the off-the-shelf DFM operates within the rated speed at rated stator flux magnitude in high-speed mode. The parameters of the DFM are given in Table II. The stator of the DFM is connected to the proposed transfer switch that can toggle the stator connection to the ac source during high-speed mode operation. The switch configuration S_{ind} is used to preselect the switched-DFM drive topology for evaluation. The drive is configured in the LSI topology if the S_{ind} is turned ON. Alternatively, the drive is configured in the LSS topology where a separate 20-V dc source supplies the stator during low-speed mode. In the transfer switch, diodes are placed in series with each SCR to enable faster turn off during mode transition. An *RC* snubber of 330 Ω and 6.8 nF is connected in parallel with the SCRs to limit the dv/dt stress. The rotor of the DFM is connected to the ac grid using a back-to-back converter configuration using two Texas Instruments High-Voltage Motor Control & PFC Developer' s Kits. The DFM is connected to a load generator (PMSG), which can operate with different load torque profiles with respect to the speed. The mode transition is initiated by a hysteresis comparator that compares the rotor speed to high and low threshold set points.

A. Performance of the Proposed Transfer Switch During Mode Transition

Fig. 12 shows the performance of the proposed transfer switch during different mode transitions. A low-speed-to-high-speed mode transition in the LSI topology is shown in Fig. 12(a)–(c). Prior to transition, the low-speed SCR-bank carries slip frequency stator current as shown in Fig. 12(b). After the transition at the zero second, the high-speed SCR-bank carries ac source frequency stator current shown in Fig. 12(c). The B- and C-phase current polarities are both positive and, therefore, a positive polarity of ac source line-to-line voltages V_{ba} and V_{ca} make the commutation of the outgoing SCRs feasible without any additional supporting circuitry as shown in Fig. 12(a). This transition condition corresponds to Fig. 3(c).

A low-speed-to-high-speed mode transition in the LSS topology is shown in Fig. 12(d)–(f). In this case, the low-speed SCR-bank carries dc current prior to transition as evident from Fig. 12(e). The B- and C-phase current polarities being negative before transition, the outgoing SCRs in each of the phases

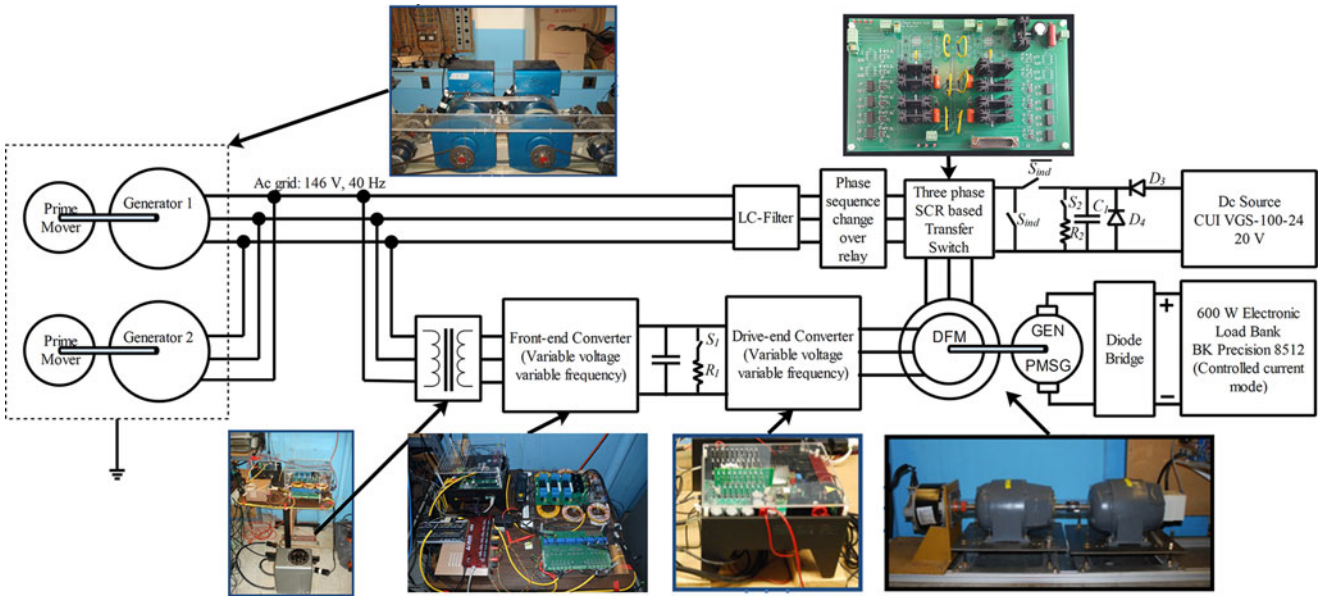

Fig. 11. Experimental setup used to evaluate the performance of the proposed transfer switch. The ac source/grid voltage and frequency levels are chosen such that the example DFM operates within the rated speed and at rated stator flux condition.

undergo natural commutation when the ac source line-to-line voltages are lesser than the negative dc source voltage as shown in Fig. 12(d).

Finally, a high-speed-to-low-speed mode transition in the LSI topology is shown in Fig. 12(g)–(i). Initially, the high-speed SCR-bank conducts the stator current at the ac source frequency, shown in Fig. 12 (h). After the transition, the stator current is commutated to the low-speed SCR-bank where the frequency changes to a lower slip frequency. At the instant of transition, current polarities in the B and C phases are both positive. Therefore, the transition is activated when the ac source line-to-line voltages $V_{\rm ba}$ and $V_{\rm ca}$ are both negative. The stator condition is precisely obtained using proper current commands to the rotor d- and q-axis currents.

B. Performance of the DFM Drive With the SCR-Based Transfer Switch

The performance of the overall switched-DFM drive under different drive torque conditions in the LSS topology is evaluated next. The drive torque command is kept constant during the low-speed-to-high-speed mode transition at six different torque magnitude levels $a-f$ as shown in Fig. 13(a). The estimated drive torque has different harmonic content in low-speed mode compared to in high-speed mode, due to the presence of harmonics in the ac source voltage. In low-speed mode, the DFM is designed to operate with the stator flux magnitude of 0.32 V·s while in high-speed mode is 0.42 V·s. The operating stator flux magnitude in high-speed mode is governed predominantly by the ac source voltage and frequency. The stator flux magnitude and the angle between the stator flux vector and the stator voltage vector δ undergoes transition at the instant of source change-over as shown in Fig. 13(b) and (c). As pointed out earlier, angle δ depends on the drive torque demand in the low-speed mode of the LSS topology while is fairly constant near 90° in the high-speed mode. The stator-flux magnitude perturbation is higher for a lower-drive torque demand as expected. This is due to the nonoptimum transition enforced by the allowable region of the ac source voltage vector location due to the SCR commutation constraint. Fig. 13(d) shows the orientation of the normalized stator flux vector and the ac source voltage vector at the instant of low-speed-to-high-speed mode transition for the six demanded drive torque cases. The stator flux vector is nearly orthogonal to the ac source voltage vector for an optimum transition for the drive torque cases $a-c$. The optimum transition instant for the ac source voltage vector falls well within the allowable constraints for the SCR commutations. However, for the remaining drive torque cases $d-f$, the ac source voltage vectors are staggered together to ensure that the SCR commutation constraints are satisfied even if the transitions happen at nonoptimum instances from the DFM perspective. A safety margin of 7° is provided to the allowable computed theoretical region of $\pm 55.5^\circ$ to ensure that the noises in the measurement and the harmonics in the source voltage do not lead to uncertainty during mode transition leading to the shorting of the sources.

Finally, the range of rotor d-axis and q-axis currents that can be supported by the proposed transfer switch while undergoing a high-speed-to-low-speed mode transition is assessed. The DFM is operated at different rotor d-axis and q-axis current combinations within the allowable rotor current limits while decelerating the drive speed as shown in Fig. 13(e). Each operating point has an uncertainty due to the measurement noise that includes the effect of switching ripple. To illustrate the uncertainty in the actual

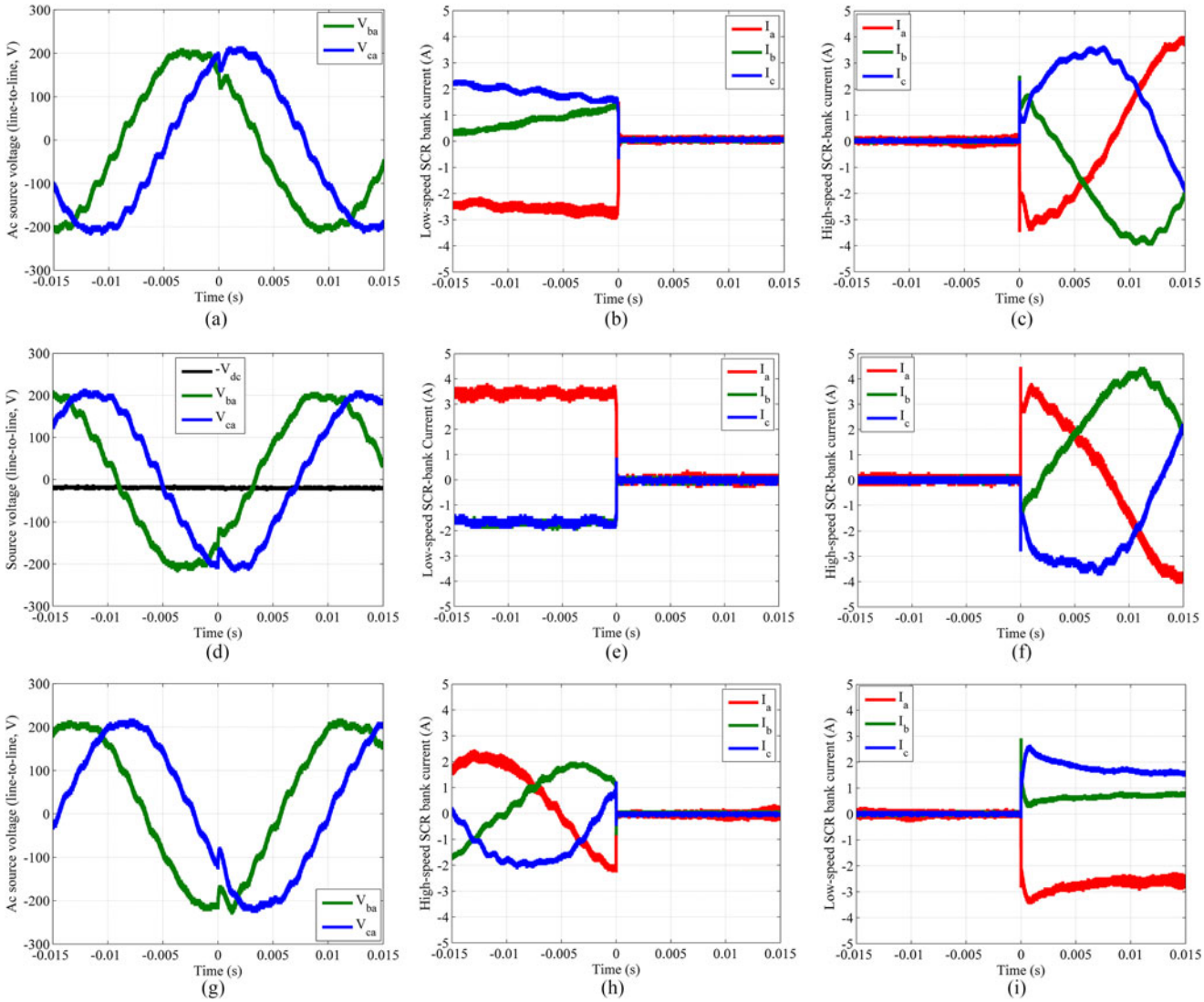

Fig. 12. Performance of the proposed transfer switch during different mode transitions. The mode-change over happens at zero second. Low-speed-to-high-speed mode transition in the LSI topology: (a) Ac source line-to-line voltage (b) low-speed SCR-bank current and the A-phase current on the shorted-side (c) high-speed SCR-bank current and the A-phase current on the ac source side. Low-speed-to-high-speed mode transition in the LSS topology: (d) Ac source line-to-line voltage and negative dc source voltage (e) low-speed SCR-bank current and the A-phase current on the dc-source side (f) high-speed SCR-bank current and the A-phase current on the ac source side. High-speed-to-low-speed mode transition in the LSI topology: (g) Ac source line-to-line voltage (h) high-speed SCR-bank current and the A-phase current on the ac source side (i) low-speed SCR-bank current and the A-phase current on the shorted-side.

operating condition, each operating point, in reality, is a circle similar to the one represent by C. The thresholds for the voltage across the incoming SCRs and the current through the outgoing SCRs are both kept at 0.1 p.u. For each of the combinations of the rotor d- and q-axis currents, the feasibility of the natural commutation of the outgoing SCRs is evaluated such that the commutation constraints are satisfied. The test result obtained is superimposed to the analytically estimated regions with the desired thresholds. As seen in Fig. 13(f), the proposed transfer switch has a wide range of operating conditions in terms of the rotor d- and q-axis currents that can simultaneously satisfy the commutation requirements of the high-speed SCR-bank. Comparatively, Fig. 13(g) shows a much smaller region of feasible natural commutation of the outgoing SCRs for the TTB transfer switch for identical threshold magnitudes.

V. Conclusion

This paper has presented and compared different topologies of solid-state transfer switches for a switched-DFM drive. The seamless transition of the DFM along with the natural commutation of the SCR-based transfer switch enables a smooth or "bumpless" mechanical operation of the switched-DFM drive over a wide range of drive torque-speed requirements. The SCR-based transfer switch along with the appropriate rotor side control enables the performance of a switched-DFM drive similar to any standard full-power converter drive. As the associated power converter for a switched-DFM drive required to handle only one-third of the shaft mechanical power over the complete speed range, the overall drive scheme becomes attractive for many high power applications including propulsion. Many variations on the transfer switch are possible, including paral-

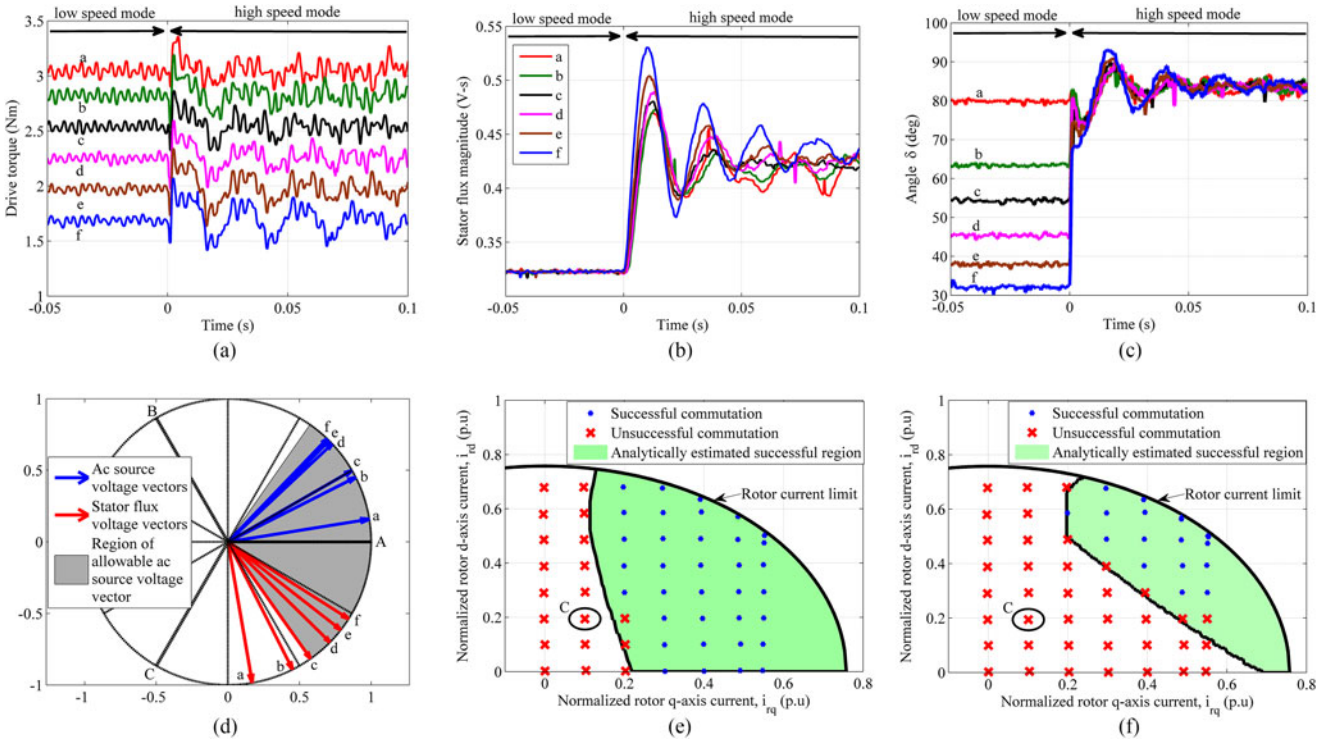

Fig. 13. Performance of the overall switched-DFM drive with the thyristor-based transfer switch. Low-speed-to-high-speed mode transition in the LSS topology for different drive torque commands: (a) estimated drive torque, (b) stator flux magnitude transition, (c) transition of the angle between the stator flux vector and the stator voltage vector, δ, (d) stator flux and ac source voltage vectors location relative to the stator ABC winding axis at the instant of mode transition. Evaluation of SCR commutation criteria during high-speed-to-low-speed mode for different combinations of rotor current components (i_{rd}, i_{rq}) with identical threshold constraints on voltage and current: (e) ETB transfer switch (f) TTB transfer switch.

lel mechanical switches or relays to reduce steady state power consumption. The analysis and design techniques in this paper can be extended to other arrangements to provide convenient transfer switch properties for any application.

REFERENCES

[1] S. Kouro, J. Rodriguez, B. Wu, S. Bernet, and M. Perez, "Powering the future of industry: High-power adjustable speed drive topologies," *IEEE Ind. Appl. Mag.*, vol. 18, no. 4, pp. 26–39, Jul. 2012.

[2] L. Parsa and H. Toliyat, "Five-phase permanent magnet motor drives for ship propulsion applications," in *Proc. IEEE Electr. Ship Technol. Symp.*, Jul. 2005, pp. 371–378.

[3] C. Lewis, "The advanced induction motor," in *Proc. IEEE Power Eng. Soc. Summer Meeting*, Jul. 2002, vol. 1, pp. 250–253.

[4] S. Muller, M. Deicke, and R. De Doncker, "Doubly fed induction generator systems for wind turbines," *IEEE Ind. Appl. Mag.*, vol. 8, no. 3, pp. 26–33, May 2002.

[5] A. Tessarolo, G. Zocco, and C. Tonello, "Design and testing of a 45-mw 100-hz quadruple-star synchronous motor for a liquefied natural gas turbo-compressor drive," *IEEE Trans. Ind. Appl.*, vol. 47, no. 3, pp. 1210–1219, May 2011.

[6] J. Sayago, T. Bruckner, and S. Bernet, "How to select the system voltage of MV drives—A comparison of semiconductor expenses," *IEEE Trans. Ind. Electron.*, vol. 55, no. 9, pp. 3381–3390, Sep. 2008.

[7] J. Rodriguez, S. Bernet, B. Wu, J. Pontt, and S. Kouro, "Multilevel voltage-source-converter topologies for industrial medium-voltage drives," *IEEE Trans. Ind. Electron.*, vol. 54, no. 6, pp. 2930–2945, Dec. 2007.

[8] J. Rodriguez, B. Wu, S. Bernet, N. Zargari, J. Rebolledo, J. Pontt, and P. Steimer, "Design and evaluation criteria for high power drives," in *Proc. IEEE Ind. Appl. Soc. Ann. Meeting*, Oct. 2008, pp. 1–9.

[9] S. Bernet, "Recent developments of high power converters for industry and traction applications," *IEEE Trans. Power Electron.*, vol. 15, no. 6, pp. 1102–1117, Nov. 2000.

[10] A. Masaoud, H. W. Ping, S. Mekhilef, and A. Taallah, "New three-phase multilevel inverter with reduced number of power electronic components," *IEEE Trans. Power Electron.*, vol. 29, no. 11, pp. 6018–6029, Nov. 2014.

[11] M. Narimani, B. Wu, Z. Cheng, and N. Zargari, "A new nested neutral point-clamped (NNPC) converter for medium-voltage (MV) power conversion," *IEEE Trans. Power Electron.*, vol. 29, no. 12, pp. 6375–6382, Dec. 2014.

[12] E. Levi, "Multiphase electric machines for variable-speed applications," *IEEE Trans. Ind. Electron.*, vol. 55, no. 5, pp. 1893–1909, May 2008.

[13] M. Darijevic, M. Jones, and E. Levi, "An open-end winding four-level five-phase drive," *IEEE Trans. Ind. Electron.*, to be published.

[14] S. Debnath, J. Qin, B. Bahrani, M. Saeedifard, and P. Barbosa, "Operation, control, and applications of the modular multilevel converter: A review," *IEEE Trans. Power Electron.*, vol. 30, no. 1, pp. 37–53, Jan. 2015.

[15] E. Cipriano Dos Santos, J. G. Muniz, E. Cabral da Silva, and C. Jacobina, "Nested multilevel topologies," *IEEE Trans. Power Electron.*, vol. 30, no. 8, pp. 4058–4068, Aug. 2015.

[16] Z. Chen, J. Guerrero, and F. Blaabjerg, "A review of the state of the art of power electronics for wind turbines," *IEEE Trans. Power Electron.*, vol. 24, no. 8, pp. 1859–1875, Aug. 2009.

[17] A. Banerjee, M. Tomovich, S. B. Leeb, and J. L. Kirtley, "Power converter sizing for a switched doubly fed machine propulsion drive," *IEEE Trans. Ind. Appl.*, vol. 51, no. 1, pp. 248–258, Jan. 2015.

[18] A. Banerjee, S. B. Leeb, and J. L. Kirtley, "Switched doubly fed machine for ship propulsion," in *Proc. Electr. Mach. Technol. Symp. ASNE*, May 2014.

[19] B. Wu, *High-Power Converters and AC Drives*. Piscataway, NJ, USA: IEEE Press, Mar. 2006.
[20] A. Banerjee, S. B. Leeb, and J. L. Kirtley, "Seamless grid interaction for a switched doubly-fed machine propulsion drive," in *Proc. IEEE Int. Electr. Mach. Drives Conf.*, May 2015, pp. 1049–1055.
[21] L. Morel, H. Godfroid, A. Mirzaian, and J.-M. Kauffmann, "Double-fed induction machine: Converter optimisation and field oriented control without position sensor," *IEE Proc. Electr. Power Appl.*, vol. 145, no. 4, pp. 360–368, Jul. 1998.
[22] S. B. Leeb, J. L. Kirtley, W. Wichakool, Z. Remscrim, C. N. Tidd, J. A. Goshorn, K. Thomas, R. W. Cox, and R. Chaney, "How much dc power is necessary?" *Naval Eng. J.*, vol. 122, no. 2, pp. 79–92, 2010.
[23] A. Banerjee, S. B. Leeb, and J. L. Kirtley, "A comparison of switched doubly-fed machine drive topologies for high power applications," in *Proc. IEEE Int. Electr. Mach. Drives Conf.*, May 2015, pp. 796–803.
[24] F. Bonnet, L. Lowinsky, M. Pietrzak-David, and P.-E. Vidal, "Doubly fed induction machine speed drive for hydro-electric power station," in *Proc. Eur. Conf. Power Electron. Appl.*, Sep. 2007, pp. 1–9.
[25] X. Yuan, J. Chai, and Y. Li, "A converter-based starting method and speed control of doubly fed induction machine with centrifugal loads," *IEEE Trans. Ind. App.*, vol. 47, no. 3, pp. 1409–1418, May 2011.
[26] A. Banerjee, A. Chang, K. Surakitbovorn, S. B. Leeb, and J. L. Kirtley, "Bumpless automatic transfer for a switched doubly-fed machine propulsion drive," *IEEE Trans. Ind. Appl.*, vol. 51, no. 4, pp. 3147–3158, Jul. 2015.
[27] A. Banerjee, M. Tomovich, S. B. Leeb, and J. L. Kirtley, "Control architecture for a switched doubly fed machine propulsion drive," *IEEE Trans. Ind. Appl.*, vol. 51, no. 2, pp. 1538–1550, Mar. 2015.
[28] A. Banerjee, S. B. Leeb, and J. L. Kirtley, "Transient performance comparison of switched doubly-fed machine propulsion drives," in *Proc. IEEE Transportation Electrification Conf. Expo.*, Jun. 2015, pp. 1–6.
[29] J. Schwartzenberg and R. De Doncker, "15 kv medium voltage static transfer switch," in *Proc. IEEE 30th IAS Ann. Meeting, Conf. Rec. IEEE Ind. Appl. Conf.*, Oct. 1995, vol. 3, pp. 2515–2520.
[30] C. Meyer, M. Hoing, and R. De Doncker, "Novel solid-state circuit breaker based on active thyristor topologies," in *Proc. IEEE 35th Annu. Power Electron. Specialists Conf.*, 2004, vol. 4, pp. 2559–2564.
[31] H. Mokhtari and M. Iravani, "Effect of source phase difference on static transfer switch performance," *IEEE Trans. Power Del.*, vol. 22, no. 2, pp. 1125–1131, Apr. 2007.
[32] B. Tian, C. Mao, J. Lu, D. Wang, Y. He, Y. Duan, and J. Qiu, "400 v/1000 kva hybrid automatic transfer switch," *IEEE Trans. Ind. Electron.*, vol. 60, no. 12, pp. 5422–5435, Dec. 2013.
[33] D. Ransom, "Choosing the correct transfer switch," *IEEE Trans. Ind. Appl.*, vol. 49, no. 6, pp. 2820–2824, Nov. 2013.
[34] Z. Liu and J. Liu, "Indirect current control based seamless transfer of three-phase inverter in distributed generation," *IEEE Trans. Power Electron.*, vol. 29, no. 7, pp. 3368–3383, Jul. 2014.
[35] P.-T. Cheng and Y.-H. Chen, "Design of an impulse commutation bridge for the solid-state transfer switch," *IEEE Trans. Ind. Appl.*, vol. 44, no. 4, pp. 1249–1258, Jul. 2008.

Arijit Banerjee (S'12) received the B.E. degree in electrical engineering from Bengal Engineering and Science University, Howrah, India, in 2005, and the M.Tech. degree in electrical engineering from the Indian Institute of Technology Kharagpur, Kharagpur, India, in 2007. He is currently working toward the Ph.D. degree at the Massachusetts Institute of Technology, Cambridge, MA, USA.

During 2006–2007, he was a Visiting Student with the Institute for Power Electronics and Control of Drives, Technische Universität Darmstadt, Darmstadt, Germany, under a German Academic Exchange Service (DAAD) Fellowship. From 2007 to 2011, he was with the Power Conversion Systems Group, General Electric Global Research Centre, Bangalore, India, where he was working on monitoring and diagnostics of electromechanical systems using electrical signatures. In 2011, he joined the Laboratory for Electromagnetic and Electronic Systems, Massachusetts Institute of Technology. He is the holder of ten issued patents and several patent applications. His research interests include analysis, design, control, and diagnostics of electromechanical systems.

Steven B. Leeb (F'07) received the doctoral degree from the Massachusetts Institute of Technology, Cambridge, MA, USA, in 1993.

He has served as a Commissioned Officer in the USAF reserves, and he has been a Member on the M.I.T. faculty, Department of Electrical Engineering and Computer Science since 1993. He also holds a joint appointment in MIT' s Department of Mechanical Engineering. He currently serves as the MacVicar Fellow and the Professor of electrical engineering and computer science in the Laboratory for Electromagnetic and Electronic Systems. In his capacity as a Professor at M.I.T, he is concerned with the design, development, and maintenance processes for all kinds of machinery with electrical actuators, sensors, or power electronic drives. He is the author or coauthor of over 80 publications and 13 US Patents in the fields of electromechanics and power electronics.

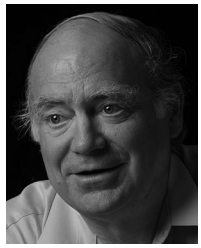

James L. Kirtley Jr. (F'91) received the Ph.D. degree from the Massachusetts Institute of Technology (MIT), Cambridge, MA, USA, in 1971.

He is the Professor of electrical engineering at MIT. He was with the Department of Large Steam Turbine Generator, General Electric, as an Electrical Engineer, with Satcon Technology Corporation as the Vice President, and the General Manager of the Tech Center and also the Chief Scientist and the Director. He was the Gastdozent at the Swiss Federal Institute of Technology.

Dr. Kirtley is a specialist in electric machinery and electric power systems. He served as an Editor-in-Chief of the IEEE TRANSACTIONS ON ENERGY CONVERSION from 1998 to 2006 and continues to serve as an Editor for that journal and as a Member of the Editorial Board of the *Journal Electric Power Components and Systems*. He was awarded the IEEE Third Millennium Medal in 2000 and the Nikola Tesla Prize in 2002. He was elected to the United States National Academy of Engineering in 2007. He is a Registered Professional Engineer in Massachusetts.